Hyperglycemia Induces Meibomian Gland Dysfunction

Yuli Guo,[1] Houjian Zhang,[1] Zhongyang Zhao,[1] Xin Luo,[1] Minjie Zhang,[1] Jinghua Bu,[1] Minghui Liang,[1] Han Wu,[1] Jingwen Yu,[1] Hui He,[1] Rongrong Zong,[1] Yongxiong Chen,[1] Zuguo Liu,[1] and Wei Li[1–3]

[1]Eye Institute of Xiamen University, Fujian Provincial Key Laboratory of Ophthalmology and Visual Science, School of Medicine, Xiamen University, Xiamen, China
[2]Department of Ophthalmology, Xiang'an Hospital of Xiamen University, Xiamen, China
[3]Xiamen University affiliated Xiamen Eye Center, Xiamen, Fujian, China

Correspondence: Wei Li, Eye Institute of Xiamen University, Fujian Provincial Key Laboratory of Ophthalmology and Visual Science, School of Medicine, Xiamen University, 4th Floor, 4221-122, South Xiang'an Rd, Xiamen, Fujian 361102, China; wei1018@xmu.edu.cn.

YG and HZ contributed equally to this work thus should be considered as co-first authors.

Received: July 15, 2021
Accepted: December 26, 2021
Published: January 24, 2022

Citation: Guo Y, Zhang H, Zhao Z, et al. Hyperglycemia induces Meibomian gland dysfunction. *Invest Ophthalmol Vis Sci.* 2022;63(1):30. https://doi.org/10.1167/iovs.63.1.30

Purpose. Patients diagnosed with diabetes are inclined to have abnormalities on stability of tear film and disorder of meibomian gland (MG). This study aims to explore the pathological change of MG induced by diabetes in a rat model.

Methods. Sprague-Dawley (SD) rats were intraperitoneally injected with streptozotocin (STZ) to establish a diabetic animal model. Lipid accumulation in MG was detected by Oil Red O staining and LipidTox staining. Cell proliferation status was determined by Ki67 and P63 immunostaining, whereas cell apoptosis was confirmed by TUNEL assay. Gene expression of inflammatory cytokines and adhesion molecules IL-1α, IL-1β, ELAM1, ICAM1, and VCAM1 were detected by RT-PCR. Activation of ERK, NF-κB, and AMPK signaling pathways was determined by Western Blot analysis. Oxidative stress-related factors NOX4, 4HNE, Nrf2, HO-1, and SOD2 were detected by immunostaining or Western Blot analysis. Tom20 and Tim23 immunostaining and transmission electron microscopy were performed to evaluate the mitochondria functional and structure change.

Results. Four months after STZ injection, there was acini dropout in MG of diabetic rats. Evident infiltration of inflammatory cells, increased expression of inflammatory factors, and adhesion molecules, as well as activated ERK and NF-κB signaling pathways were identified. Oxidative stress of MG was evident in 4-month diabetic rats. Phospho-AMPK was downregulated in MG of 2-month diabetic rats and more prominent in 4-month rats. After metformin treatment, phospho-AMPK was upregulated and the morphology of MG was well maintained. Moreover, inflammation and oxidative stress of MG were alleviated after metformin intervention.

Conclusions. Long-term diabetes may lead to Meibomian gland dysfunction (MGD). AMPK may be a therapeutic target of MGD induced by diabetes.

Keywords: diabetes, Meibomian gland, AMPK, inflammation, oxidative stress

Meibomian glands (MGs) are located on the superior and inferior tarsal plates.[1] Meibocytes secrete meibum through holocrine to the ocular surface, where it lubricates the ocular surface, sustains tear film stability to prevent tear evaporation, and contributes to form a barrier between the ocular surface and microbe.[2,3] Therefore, MGs play a pivotal role in maintaining ocular surface homeostasis. Meibomian gland dysfunction (MGD) is a group of chronic functional abnormalities of MGs, featured by hyposecretion/ hypersecretion or obstruction of MGs, the quality/quantity alterations of meibum and eventual acinar atrophy and gland dropout.[4] MGD often results in damage of tear film stability and ultimate evaporative dry eye, which compromises the life quality of patients with dry eye.[5]

Besides age and environmental stress, systemic factors can also conduce to MGD. Numerous clinical studies have indicated the correlation between MGD and systemic factors, such as androgen deficiency,[6] hyperlipidemia,[7] and so on. As a group of metabolic disorders, diabetes mellitus (DM) has also been observed as a systemic risk factor for MGD.[8] Diabetes is a public health problem and its ocular complications, such as diabetic retinopathy, cataract, and orbital infections, can cause blindness.[9] The ocular surface is known to be involved in diabetes in various ways, such as dry eye,[10] recurrent corneal erosions,[11] etc. Several studies demonstrated that patients diagnosed with diabetes might predispose to MG disorders.[12–15] Compared with nondiabetic patients, the patients with diabetes displayed more undesirable MG parameters.[12] Moreover, MG dropouts could be found evidently in patients with diabetes.[13] In addition, an in vitro experiment proved that high glucose is detrimental for human MG epithelial cells.[16] These findings suggested that MGD may be related to hyperglycemia. However, the pathological process of MGD caused by diabetes still remains ambiguous. In this study, we explored the pathological change of MGs induced by diabetes with a diabetic rat model and explicate the association of MGD with hyperglycemia, which may shed new light

on clinical diagnosis and treatment of MGD caused by diabetes.

Materials and Methods

Materials

Rabbit anti-collagen IV (ab6586), anti-peroxisome proliferator-activated receptor (PPARγ; ab45036), anti-Ki67 (ab16667), anti-p63 (ab124762), anti-K10 (ab76318), anti-sprr1b (ab123237), anti-NADPH oxidase 4 (NOX-4, ab133303), anti-heme oxygenase 1 (HO-1, ab13243), anti-superoxide dismutase 2 (SOD2, ab13533), and anti-4 Hydroxynonenal (4-HNE, ab46545) antibodies were from Abcam (Cambridge, UK). Rabbit anti-NF-κB p65 (Cat #8242), anti-phospho-NF-κB p65 (Cat #3033), anti-ERK1/2 (Cat #4695S), anti-phospho-ERK1/2 (Cat #9101S), and anti-phospho-AMPKα (Cat #2535S) antibodies were from Cell Signaling Technology (Danvers, MA, USA). Rabbit anti-NF-E2-related factor2 (Nrf2, 16396-1-AP), anti-Tom20 (11802-1-AP), and anti-Tim23 (11123-1-AP) antibodies were from Proteintech (Chicago, IL, USA). Rabbit anti-CD45 (sc-25590) and anti-AMPKα (sc-25792), antibodies were from Santa Cruz (Dallas, TX, USA). Rabbit anti-PMN (20R-PR020) antibody was from Fitzgerald (Acton, MA, USA). Alexa Fluor 594-conjugated IgG (A11058) and Alexa Fluor 488-conjugated IgG (A11055 and A21206) were from Invitrogen (Eugene, OR, USA). Horseradish peroxidase (HRP)-conjugated anti-β-actin antibody (a5316) and dihydroethidium (DHE; D7008) were from Sigma-Aldrich (St. Louis, MO, USA). The 40,6-diamidino-2-phenylindole (DAPI; H-1200) and mounting medium (H-5000) were from Vector (Burlingame, CA, USA).

Animals

Male Sprague-Dawley (SD) rats (8–10 w, 180–200 g) were randomly divided into control group (NT, the no-treatment group) and an experimental group (DM, the diabetes mellitus group). Rats of experimental groups were intraperitonially injected with streptozotocin (STZ; Sigma; 65 mg/kg) to induce diabetes using the previous protocol.[17] All studies were performed in accordance with the Association for Research in Vision and Ophthalmology (ARVO) Statement for the Use of Animals in Ophthalmic and Vision Research with the approval of the Animal Ethical Committee of Xiamen University (approval No. XMULAC20170014). Animals were given free access to standard rodent chow and water and kept in a standard pathogen-free environment at 25°C $\pm$ 1°C, relative humidity 55% $\pm$ 5%, and alternating 12 hours of light-dark cycles (lights on at 8:00 and lights off at 20:00). In another experiment, rats were randomly divided into three groups: a control (NT) group, a DM group (65 mg/kg STZ injection, normal saline gavage was applied daily from 2 months after STZ injection), and a metformin (Met; YEASEN, China) group (65 mg/kg STZ injection, 700 mg/kg metformin gavage was applied daily from 2 months after STZ injection for 2 months). The animals were euthanized at different time points from 1 week to 4 months after modeling.

Animal Examination

All the animals were weighed and tested the blood glucose level at 2 weeks, 2 months, and 4 months after STZ injection. Then the eyelid margins and corneas were observed and imaged on a slit-lamp microscope (Kanghua Science & Technology Co. Ltd., Chongqing, China) by a single ophthalmologist. After euthanization of the animal, the upper and lower eyelids were excised en bloc and the MGs were dissected by removing the eyelid skin and underneath orbicularis oculi muscles. The MG structure was then observed and photographed with a stereoscopic zoom microscope (Leica M165-FC; Germany).

Transmission Electron Microscopy

MG specimens were immediately fixed after euthanization by immersing them in 2.5% glutaraldehyde in 0.1 M PBS (pH 7.4) for 4 hours at 4°C. The samples were then washed 3 times with 0.1 M PBS solution, postfixed in 2% osmium tetroxide, dehydrated using standard series of ethanol and propylene oxide concentrations, then embedded in epoxy resin. One-micrometer sections were stained with methylene blue and MG tissues were then thin sectioned on an ultramicrotome (LKB, Gaithersburg, MD, USA). Sections were collected on 150-mesh grids, stained with uranyl acetate and lead citrate, examined, and photographed using a transmission electron microscope (model 1200 EXII; JEOL, Tokyo, Japan)

Histology

Eyelid tissues collected from control and diabetic rats were embedded in optimal cutting temperature (OCT) compound or paraffin, cut into sagittal sections (6 µm thick), and then stored at −80°C (frozen sections) or room temperature (paraffin sections). Paraffin sections were prepared for immunohistochemical staining and hematoxylin and eosin staining, whereas immunofluorescence staining and Oil Red O staining and LipidTox staining were performed on frozen sections.

Oil Red O Staining

Frozen eyelid sections were fixed in 4% paraformaldehyde for 10 minutes, washed in PBS for 5 minutes, and stained for 10 minutes in freshly prepared Oil Red O solution. After rinsing with PBS for 5 minutes, the sections were counterstained with hematoxylin and mounted in 90% glycerol.

LipidTOX Staining

Frozen eyelid sections were fixed in 4% paraformaldehyde for 10 minutes, rinsed in PBS for 5 minutes, diluted the LipidTOX neutral lipid stain (H34475; Thermofisher, Waltham, MA, USA) 1:200 in buffer and incubated the sections at room temperature for at least 30 minutes, followed by counterstaining with DAPI. Sections were then evaluated and imaged with a microscope (DM2500; Leica Microsystems, Wetzlar, Germany).

Immunofluorescence Staining

For immunofluorescence staining, sections were fixed in paraformaldehyde at room temperature for 10 minutes followed by washing 3 times using PBS for 5 minutes each. Sections were incubated with 0.2% Triton X-100 for 20 minutes and again washed 3 times with PBS

Investigative Ophthalmology & Visual Science

for 5 minutes each. Tissue sections were then blocked with 2% BSA in PBS for 60 minutes at room temperature and incubated with collagen IV (1:500, 2 µg/mL), PPAR-γ (1:100, 10 µg/mL), Ki67 (1:100, 0.29 µg/mL), p63 (1:300, 2.72 µg/mL), K10 (1:100, 3.78 µg/mL), Sprr1b (1:100, 1 µg/mL), CD45 (1:100, 2 µg/mL), PMN (1:1200, 1 µg/mL), Tom20 (1:200, 2 µg/mL), and Tim23 (1:200, 2 µg/mL) antibodies for 16 hours at 4°C. Negative controls were performed by incubating a section with irrelevant isotype without the primary antibody (Supplementary Figs. S2A–J). The slides were then washed 3 times with PBS for 10 minutes per wash and incubated with Alexa Fluor 594-conjugated IgG (1:300, 3.3 µg/mL) or Alexa Fluor 488-conjugated IgG (1:300, 3.3 µg/mL) for 60 minutes at 37°C, followed by counterstaining with DAPI. Sections were then evaluated and imaged with a microscope (DM2500; Leica Microsystems, Wetzlar, Germany). The mean intensity of staining in some sections was measured by image analysis software (Image J, version 1.8.0.), which recognized the integrated fluorescent density of the set area, and then calculated the mean value of fluorescent density in this area.

Immunohistochemical Staining

Paraffin sections were rehydrated and blocked with 3% hydrogen peroxide for 10 minutes, followed by washing 3 times with PBS for 5 minutes each. Sections were subsequently treated with 0.2% Triton X-100 for 20 minutes. After washing 3 times each with PBS for 5 minutes, they were incubated with 2% BSA for 60 minutes, followed by incubation with NOX-4 (1:250, 8.7 µg/mL), 4-HNE (1:200, 3.35 µg/mL), and phospho-AMPKα (1:100) antibodies at 4°C for 16 hours. Negative controls were performed by incubating a section with irrelevant isotype without the primary antibody (Supplementary Figs. S3A–C). After that, the sections were rinsed 3 times with PBS for 10 minutes each, and further incubated with biotinylated anti-rabbit IgG (1:50) for 60 minutes, followed by Vectastain Elite ABC reagent for 30 minutes. The reaction product was then developed with diaminobenzidine (DAB) for 1 minute, mounted with mounting medium, and examined under a light microscope (Eclipse 50i; Nikon, Tokyo, Japan). Positively stained cells in the MGs were counted using NIS Elements image analysis software (NIS Elements version 4.1; Nikon, Melville, NY, USA).

TUNEL Assay

TUNEL assay was performed by the DeadEnd Fluorometric TUNEL System (Promega, G3250). Frozen MG sections were rehydrated and incubated with Proteinase K Tris/HCL, pH = 7.4 (10 mM) for 30 minutes at 37°C. After washing 3 times each with PBS for 5 minutes, 50 µL of TUNEL reaction mixture was added on the sections and the sections placed in the dark for 1 hour at 37°C, followed by rinsing 3 times with PBS for 5 minutes each. Finally, the specimens were counterstained with DAPI, mounted, and photographed with a microscope (DM2500; Leica Microsystems).

Dihydroethidium Staining

Freshly prepared frozen slices were incubated with 3 µmol/L DHE in a humidified chamber and protected from light (at 37°C incubator for 45 minutes). Photographs and the fluorescence intensity were analyzed with Image Image-Pro Plus 6.0 software (Media Cybernetics, Silver Spring, MD, USA).

RNA Extraction and Quantitative RT-PCR

MGs were isolated under a dissecting microscope after removal of skin, subcutaneous tissue, muscle, and palpebral conjunctiva of the animal. Total RNA was extracted from MGs using Trizol Reagent (15596018; Invitrogen). RNA sample parameters and concentrations were detected by a Du 800 Nucleic Acid/protein Analyzer (Beckman Coulter, Indianapolis, IN, USA). Five samples were used in each group, and one sample consisted of pooled MGs of both eyes of the same animal. The equal amount of RNA was reverse transcribed to cDNA using a reverse transcription kit (RR047A; TaKaRa, Shiga, Japan). Quantitative Real-Time PCR (qRT-PCR) was performed with a StepOneTM Real-Time PCR detection system (Applied Biosystems, Alameda, CA, USA) using a SYBR Premix Ex Taq Kit (RR420A; TaKaRa). The Table provides the primer sequences used to amplify specific gene products. The thermal profile used was as follows: 95°C for 10 minutes, followed by denaturation at 95°C for 10 seconds, and annealing and extension at 60°C for 30 seconds for 40 cycles. The results of qRT-PCR were analyzed by the comparative CT method and normalized with β-actin as an endogenous reference, and calibrated against the normal control group.

Table. Primer Sequences for the Quantitative Real-Time PCR.

Gene	Forward Primer (5′-3′)	Reverse Primer (5′-3′)
Elovl3	GGAGTACTGGGTAAGCTCGT	CCCATTGTAAACAGCACGGT
Soat1	CTGCATCTCTGGACAATGGC	GGTCCACTTCAAACAGCTCG
Dhcr24	GGATGGCTCACTGTCTCACT	AGGTCATCGAGTTCAGGCAA
Hmgcr	TTTCGTCTTCAGCACTGTCG	CCATCCCACGCGCTATATTC
Pparg	TGAAGACATCCCGTTCACAA	ACCCTTGCATCCTTCACAAG
Il1a	TCAAAGATGTCCACCTTCACC	CTGATCTGGGTTGGATGGTC
Il1b	CTGCAGGCTTCGAGATGAAC	TGTGCCGTCTTTCATCACAC
Sele(ELAM-1)	GCTGTGAAAGGGGCTATGTG	TGCACGTTGTATTCCATGGG
Icam1	TGCTTTGAGAACTGTGGCAC	ACTACTGAGAGCTGTGTCCG
Vcam1	TTCTGACCATGGACCCTGTC	AAACACTTGACCATGACCGG
Krt10	CGGGATCTGGAAGAGTCAAA	CGCAGGGCTACTTCATTCTC
Sprr1b	GAGTTCCCATCAGCAAAAGC	GGTGTCACAGGGCTCAGG
Actb	TGTCACCAACTGGGACGATA	GGGGTGTTGAAGGTCTCAAA

Investigative Ophthalmology & Visual Science

Western Blot Analysis

Isolated MGs were extracted in a cold lysis buffer composed of protease and phosphatase inhibitors. Protein concentration was measured by BAC protein assay kit (Cat #23225; ThermoFisher Scientific). Three samples were used in each group. Equal amounts of protein extracts (20 µg) were subjected to electrophoresis on 10% acrylamide gels and then electronically transferred to polyvinylidene difluoride (PVDF) membranes. After blocking in 5% BSA for 1 hour, the membranes were incubated overnight at 4°C with primary antibodies for anti-PPARγ (1:500, 2 µg/mL), p-ERK1/2 (1:1000, 0.084 µg/mL), ERK1/2 (1:1000, 0.191 µg/mL), NF-κB p65 (1:1000, 0.208 µg/mL), phospho-NF-κB p65 (1:1000, 0.057 µg/mL), Nrf2 (1:1000, 0.7 µg/mL), HO-1 (1:1000, 1 µg/mL), SOD2 (1:1000, 1 µg/mL), Tom20 (1:1000, 0.4 µg/mL), Tim23 (1:1000, 0.4 µg/mL), AMPKα (1:1000, 0.2 µg/mL), and phospho-AMPKα (1:1000, 0.027 µg/mL). After 3 washes with Tris buffered saline containing 0.05% Tween-20 for 10 minutes each, the membranes were incubated with HRP-conjugated goat anti-mouse or anti-rabbit IgG secondary antibodies. HRP-conjugated mouse anti–β-actin was used for protein quantification. The results were detected by enhanced chemiluminescence reagent (ECL-500; ECL, Lulong Inc., Xiamen, China) and recorded by the transilluminator (ChemiDoc XRS System; Bio-Rad, Philadelphia, PA, USA).

Statistical Analysis

GraphPad Prism version 7.0 software (GraphPad Software Inc., San Diego, CA, USA) was applied for data processing. For quantification, all data levels were given as a.u. ± STDev. Statistical analysis was performed using the unpaired Student's *t*-test to compare the differences in body weight, blood glucose, relative mRNA expression, cell counting, and gray-scale analysis. A value of $P < 0.05$ was considered statistically significant.

Results

The Manifestation of Eyelid and Ocular Surface of Diabetic Rats

The SD rats were conducted observation at regular time points of 2 weeks, 2 months, and 4 months after STZ injection within the period of 4 months after STZ intraperitonially injection. Compared with the NT group, the body weight of the DM group displayed a gradual decrease within 4 months (Fig. 1A). Meanwhile, the blood glucose level in the DM group was much higher than that of NT group at each time points (Fig. 1B), indicating availability of the DM animal model.

There was no evident change of ocular surface in the NT group and the DM group from 2 weeks to 2 months under slit-lamp microscope (Fig. 1C). On the fourth month, condensed lipid deposition at the orifice of the MG of the DM group was observed (see Fig. 1C, black arrow). Stereoscopic microscope images revealed MG dropouts with disorganized acini and ducts in 4-month DM rats (Fig. 1D, black arrow). To further determine MG morphology, H&E staining of MG was performed. Normal MG acini are spherical and plump, which maintain foam-like structure as observed in the MG sections of the NT group. However, the MG section of the 4-month DM group showed disarranged acini (Fig. 1E, black arrow), destroyed basement membrane of acini (Fig. 1G, white arrow), and decreased size of acini (see Fig. 1E, black circle), which was further identified by quantification of axis of acini (Fig. 1F).

Meibomian Gland Lipid Metabolism Disorder in Diabetic Rats

Meibomian lipids synthesized by acini are essential for the maintenance of ocular surface health and integrity.[18] Lipid metabolism disorder is one of the most common characteristics of MGD.[4] ORO staining was applied to clarify the lipid distribution in the MG tissue. It revealed that the MG of the 4-month DM group presented more condensed staining than the NT group, whereas the MG of the 2-week and 2-month DM group showed similar lipid distribution with the NT group (Fig. 2A). LipidTOX staining of MG also indicated the obvious lipid accumulation in MG of 4-month DM rats (Fig. 2B) and was confirmed by quantification of mean fluorescent intensity (Fig. 2C).

Lipidomic analysis of the meibum has been reported that enzymes involved in the fatty acid elongation cycle play a critical role in meibogenesis.[19] Elvol3 is one of such enzymes which catalyzes the elongation of C18 saturated and monounsaturated FAs to form the C20 to C24 family.[20] The qRT-PCR revealed that Elvol3 mRNA expression was transiently upregulated in the DM group at 2 weeks and then markedly downregulated in the 2-month and 4-month DM groups (Fig. 2D). As the important participants involved in the process of cholesterol production,[21] sterol O-acyltransferase-1(SOAT1) expression significantly decreased in the 2-month and 4-month DM groups (Fig. 2E), other lipid synthesis related genes 3β-Hydroxysteroid-Δ24 reductase (DHCR24; Fig. 2F) and 3-Hydroxy-3-methyl-glutaryl-coenzyme A reductase (HMGCR; Fig. 2G) expression showed mild change in MG of DM rats.

As the major subtype of the PPAR family expressed in adipocyte and sebocyte, PPAR-γ regulates the expression of genes involved in lipogenesis.[22] Normally, PPAR-γ proteins show a distinct cytoplasmic and nuclear localization in young individuals and predominant nuclear staining in old individuals.[23,24] Immunofluorescence staining of PPAR-γ showed both cytoplasmic and nuclear staining in the 2-month and 4-month NT groups, whereas the majority of meibocytes in the 2-month DM rats showed nuclear staining with decrease of PPAR-γ fluorescence intensity, and became more obvious in the 4-month DM rats (Fig. 2I). The qRT-PCR further confirmed reduced PPAR-γ gene expression in the 4-month DM group (Fig. 2H). Western blot analysis also showed the prominent decrease of PPAR-γ expression in MG of 4-month DM rats (Fig. 2J), which was confirmed by gray-scale analysis (Fig. 2K).

Abnormal Differentiation and Increased Apoptosis of MG Cells in Diabetic Rats

To determine the proliferation of MG cells, we performed immunofluorescence staining on Ki67 and p63, two proliferation related markers. There was obvious decrease of Ki67 positive cells in the basal layer of acini at the 4-month DM group (Fig. 3A), which was confirmed by cell counting (Fig. 3B). The expression of p63 distributes in basal epithelial cells of normal acini, which symbolizes the high

Investigative Ophthalmology & Visual Science

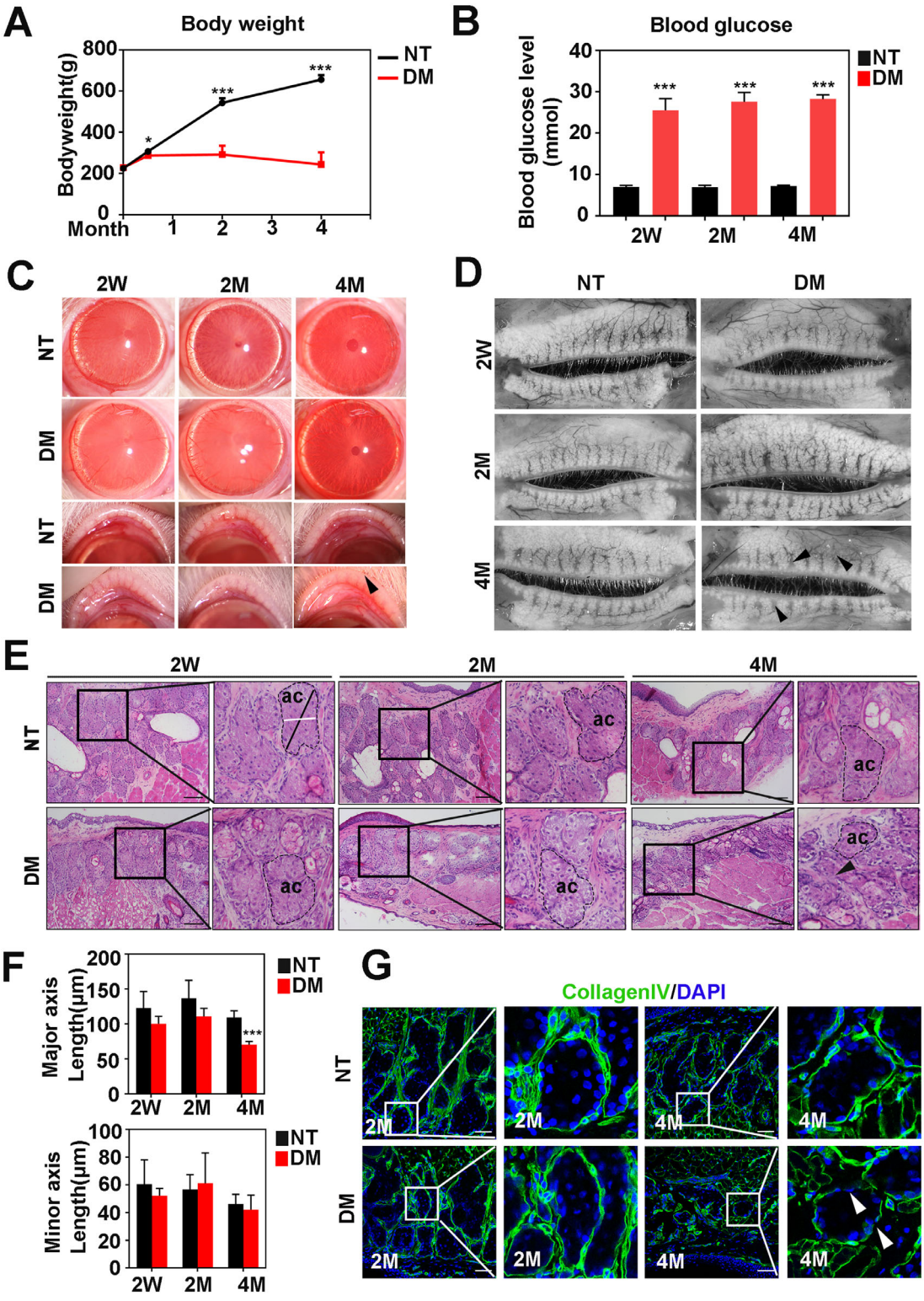

Figure 1. The manifestation of eyelid and ocular surface of DM rats. (**A**) The body weight of the DM group shows an obvious decrease compared with NT group from 2 weeks after modeling ($n = 6$). (**B**) The blood glucose level of DM group shows significant increase than the NT group at each time points ($n = 6$). (**C**) The slit lamp images of ocular surface and eyelid at 2 weeks, 2 months, and 4 months after STZ injection. The black arrow shows abnormal lipid secretion in the meibomian gland orifice. (**D**) The stereoscopic images of the meibomian gland shows the obvert MG dropout in the 4-month DM group (*black arrow heads*). (**E**) H&E staining shows disarranged MG acini (*black arrowhead*) at 4 months after STZ injection. (**F**) The quantification of length of major axis and minor axis of acini shows decreased size of acini at 4 months after STZ injection ($n = 6$). ***$P < 0.001$. Scale bars represent 200μm. (**G**) The immunofluorescent staining of collagen IV in the MG of each group. *White arrowheads* show the destroyed acini basement membrane in the MG of 4-month DM rat. Scale bars represent 100 μm.

Investigative Ophthalmology & Visual Science

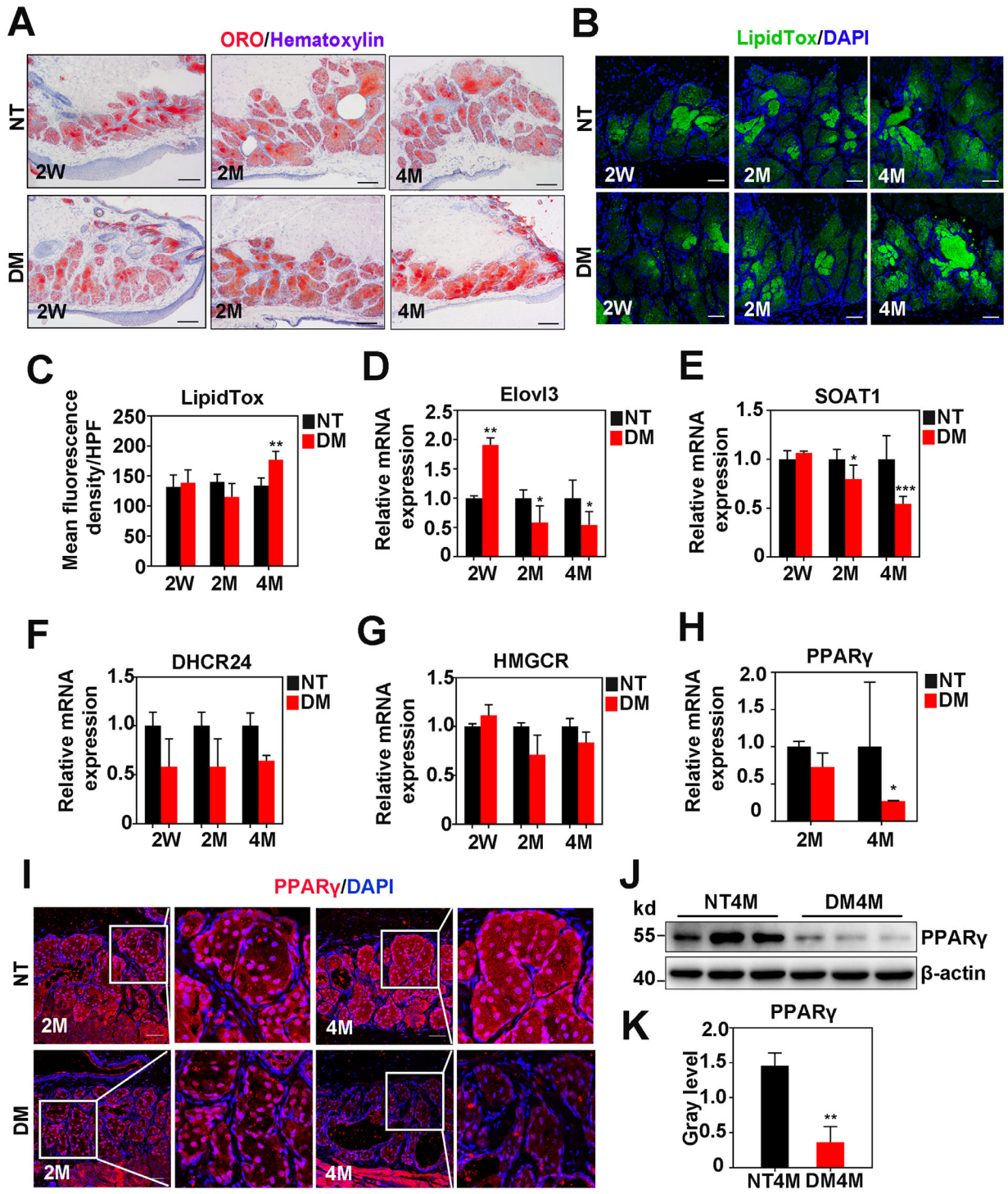

Figure 2. Lipid metabolism disorder of MG in 4-month DM rats. (**A**) The ORO staining of the MG shows condensed positive staining in 4-month DM rats. (**B**) The LipidTOX staining of the MG manifests an obvious lipid accumulation in 4-month DM rats. (**C**) The mean fluorescent intensity of LipidTOX ($n = 4$). (**D–G**) The relative mRNA expression of lipid metabolism related enzymes Elovl3, SOAT1, DHCR24, and HMGCR ($n = 6$). (**H**) The qRT-PCR shows reduced PPAR-γ mRNA expression at the MG of 4-month DM rats ($n = 6$). (**I**) The immunofluorescent staining shows reduced nuclear and cytoplasmic PPAR-γ expression at 4-month DM rats ($n = 3$). (**J**) The Western blot analysis of PPAR-γ in 4-month NT rats and DM rats. (**K**) The gray-scale analysis of Western blot shows a decrease of PPAR-γ expression at the MG of 4-month DM rats ($n = 3$). *$P < 0.05$, **$P < 0.01$, ***$P < 0.001$. Scale bars represent 200 µm in **A** and 100 µm in **B**, and **I**.

progenitive and proliferative ability.[25] The p63 positive cells were dramatically reduced in the 2-month and 4-month DM groups compared with the NT group (Figs. 3C, 3D). We further performed TUNEL staining to detect apoptotic cells and found that there were abundant apoptotic cells accumulated in the MG of 2-month and 4-month DM rats (Fig. 3E),

Investigative Ophthalmology & Visual Science

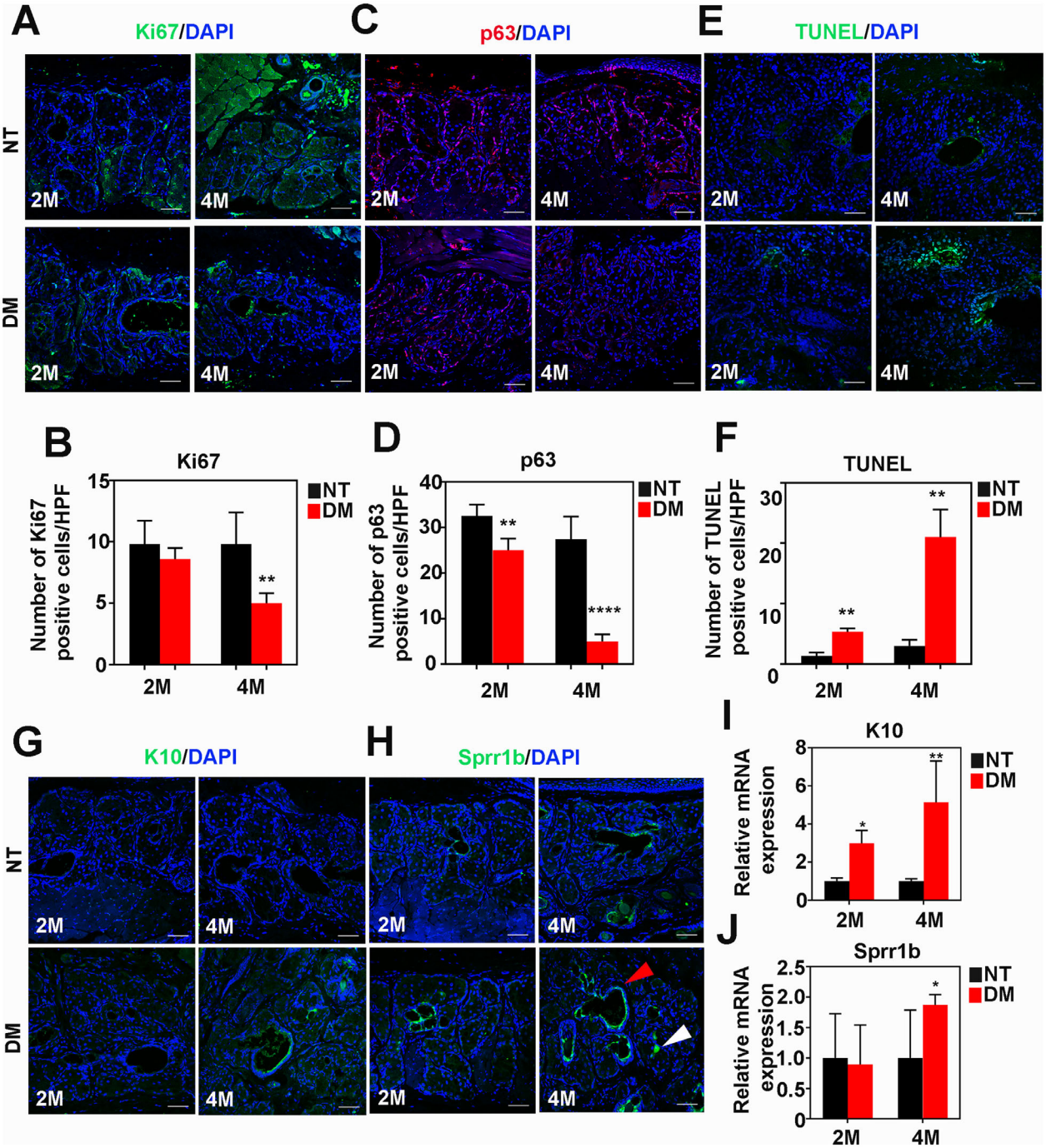

Figure 3. Abnormal differentiation and increased apoptosis of MG cells in 4-month DM rats. (**A**) Immunofluorescent staining of Ki67 shows positive staining in the acini of the MG. (**B**) Ki67 positive cell counting shows a significant decrease in the 4-month DM group ($n = 5$). (**C**) Immunofluorescent staining of p63 shows positive staining in the acini of the MG. (**D**) Quantification of p63 positive cells shows decrease in the 2-month DM group and the 4-month DM group ($n = 5$). (**E**) TUNEL staining demonstrates apoptotic cells in the MG. (**F**) Quantification of TUNEL positive cells shows an increase in the 2-month DM group and the 4-month DM group ($n = 3$). (**G**) Immunofluorescent staining of K10 shows keratinization of epithelial cells in the MG. (**H**) Immunofluorescent staining of Sprr1b in the MG of each group. (**I**) The relative mRNA expression shows an obvious increase of K10 in the 4-month DM group ($n = 6$). (**J**) The relative mRNA expression shows an obvious increase of Sprr1b in the 4-month DM group ($n = 4$). $^{*}P < 0.05$, $^{**}P < 0.01$, $^{***}P < 0.001$. Scale bars represent 100 µm in **A**, **C**, **E**, **G**, and **H**.

which was further confirmed by cell counting (Fig. 3F). However, we did not detect apoptotic cells in MG at 1 week and 2 weeks after STZ application (Supplementary Fig. S1A). These results indicate that proliferation decrease and apoptosis increase of MG cells happened at the late stage of hyperglycemia rather than early stage of the diabetic rat model.

Hyper-keratinization, a typical pathological alteration of obstructive MGD, implies the abnormal differentiation of ductal epithelial cells, which is the initial factor of

degenerative gland dilatation and atrophy.[26,27] Immunofluorescence staining of K10, which is the marker for the terminally keratinized epithelium,[28] showed increased intensity in the duct of 4-month DM group (Fig. 3G), verified by qRT-PCR (Fig. 3I). Overexpression of small proline-rich protein 1b (Sprr1b) in MG denotes squamous metaplasia.[29] In the 4-month DM group, we detected increased expression of Sprr1b in both ducts (Fig. 3H, red arrow) and acini (see Fig. 3H, white arrow), which was also confirmed by qRT-PCR (Fig. 3J). We also detected the morphology and K10 expression of the cornea of the 4-month DM group. However, the cornea of the 4-month DM group was well-maintained and the immunofluorescent staining did not detect positive K10 expression in cornea of 4-month DM group (Supplementary Figs. S4A–D), indicating that there was still no obvious keratinization in the cornea in the 4-month DM rats albeit significant keratinization in MG.

Inflammation of MG in Diabetic Rats

To further evaluate inflammation in MG of DM rats, we detected the distribution of CD45 and PMN positive cells in MG by immunohistochemical staining. Compared with the NT group, MG of the 4-month DM group displayed local accumulation of inflammatory cells around the acini, which was more explicit with enumeration of positive cells (Figs. 4A–D). The mRNA expression of inflammatory cytokines and adhesion molecules, such as IL-1α, IL-1β, ELAM1, ICAM1, and VCAM1, manifested a prominent increase in MG of the 4-month DM group (Figs. 4E–I). Extracellular signal-regulated kinase (ERK) is a member of the mitogen-activated protein kinase family of signaling molecules, which has been proved to be implicated in chronic inflammation.[30] Western blot analysis revealed that the protein expression of both two phosphorylated forms of ERK, pERK1 (p-p44) and pERK2 (p-p42), were notably upregulated in the MG of 4-month DM rats (Fig. 4J), which was quantified by gray-scale analysis (Fig. 4K). As the master regulator of inflammation, NF-κB plays a vital role in inflammation responses.[31] According to the result of the Western blot analysis, the phosphorylation level of NF-κB p65 in the MG of the 4-month DM group had a conspicuous increase compared with the NT group (see Fig. 4J), affirmed by gray-scale analysis (see Fig. 4K).

Oxidative Stress and Mitochondria Deterioration of MG in Diabetic Rats

Oxidative stress, an imbalance between oxidative and antioxidative systems of cells and tissues, is a result of over production of associated reactive oxygen species (ROS), which is the prominent characteristic of diabetes.[32] We utilized DHE to detect in situ production of ROS and found that ROS was increased in the MG of the 2-month DM group and there was overt accumulation of ROS in acini in the 4-month DM group (Fig. 5A), which was verified by quantification of fluorescence intensity (Fig. 5B). The nicotinamide adenine dinucleotide phosphate (NADPH) oxidase subunit 4 (NOX4) is a substrate of NADPH that can generate ROS.[33] Immunohistochemical staining showed that NOX4 nuclear and cytoplasmic staining was significantly increased in the MG of the 4-month DM group (Fig. 5C), confirmed by quantification of mean gray value (Supplementary Data 3D). An obvious increase of lipid peroxidation derived 4-hydroxynonenal (4-HNE) cytoplasmic staining was also observed in MG of 4-month DM group (Fig. 5D, see Supplementary Fig. S3E). With respect to anti-oxidation factors, inversely, the protein expression of nuclear factor erythroid-2 related factor-2 (Nrf2), heme oxygenase-1 (HO-1), and superoxide dismutase (SOD2) were visibly downregulated in the 4-month DM group (Fig. 5E), and was confirmed by quantitative gray-scale analysis (Figs. 5F–H).

Mitochondria is the main source of ROS.[34] It was well established that structure of mitochondria can be damaged by excessive ROS.[35] We then determined mitochondrial outer membrane protein Tom20 and inner membrane protein Tim23 expression by immunofluorescent staining and Western blot analysis. There was an evident decrease of fluorescent intensity of Tom20 (Fig. 5I) and Tim23 (Fig. 5J) in acini of the 4-month DM group, Western blot analysis also showed an obvious decrease in the MG of the 4-month DM group (Fig. 5K), which was confirmed by quantitative gray-scale analysis (Figs. 5L, 5M). To further observe the morphology of the mitochondria of MG acinar cells, transmission electron microscope (TEM) was applied. TEM images revealed that mitochondrial inner and outer membrane of the MG acinar cells were well-maintained in the 2-month NT group, the 2-month DM group (see Supplementary Fig. S4G), and the 4-month NT group (Fig. 5N, white arrows), whereas they displayed a heteromorphic morphology in the 4-month DM group (Fig. 5N, black arrow).

Inactivation of AMPK in the MG of Diabetic Rats

The 5′-adenosine monophosphate-activated protein kinase (AMPK) is a crucial cellular bioenergetic sensor which participates in a plethora of cellular functions ranging from inflammation, oxidative stress to apoptosis.[36] As the upstream modulator of various biological processes, AMPK suppression is found to be evident in various tissues and organs in diabetes.[37] To further elucidate the role of AMPK in the pathology of MGD induced by hyperglycemia, we identified the distribution of phospho-AMPKα by immunohistochemical staining and protein expression of phospho-AMPKα by Western blot analysis. The results showed that phospho-AMPKα was dramatically decreased in acini as early as in the 2-month DM group (Fig. 6A), which was verified by Western blot analysis and quantitative gray-scale analysis (Figs. 6B, 6C). These results suggested that AMPK was downregulated in the MG of DM rats, indicating activation of AMPK might protect the MG from MGD induced by hyperglycemia.

AMPK Agonist Treatment Protects the MG from Pathological Exacerbation in Diabetic Rats

As an efficient AMPK agonist, metformin shows pronounced effects on activation of AMPK signaling.[38] To determine whether AMPK agonist can protect the MG of DM, metformin was applied by gavage in 2-month DM rats and lasted for 2 months. First, we investigated the dose dependency of metformin in rat MG tissues. We found phospho-AMPKα was activated in the MG at 700 mg/kg daily gavage (Fig. 6D), which is comparatively higher than the usual dose in other tissues or organs.[39–41] We monitored the blood glucose levels of the three groups during the DM duration, and the result showed that there was no significant drop of blood glucose level after Met treatment (see

Investigative Ophthalmology & Visual Science

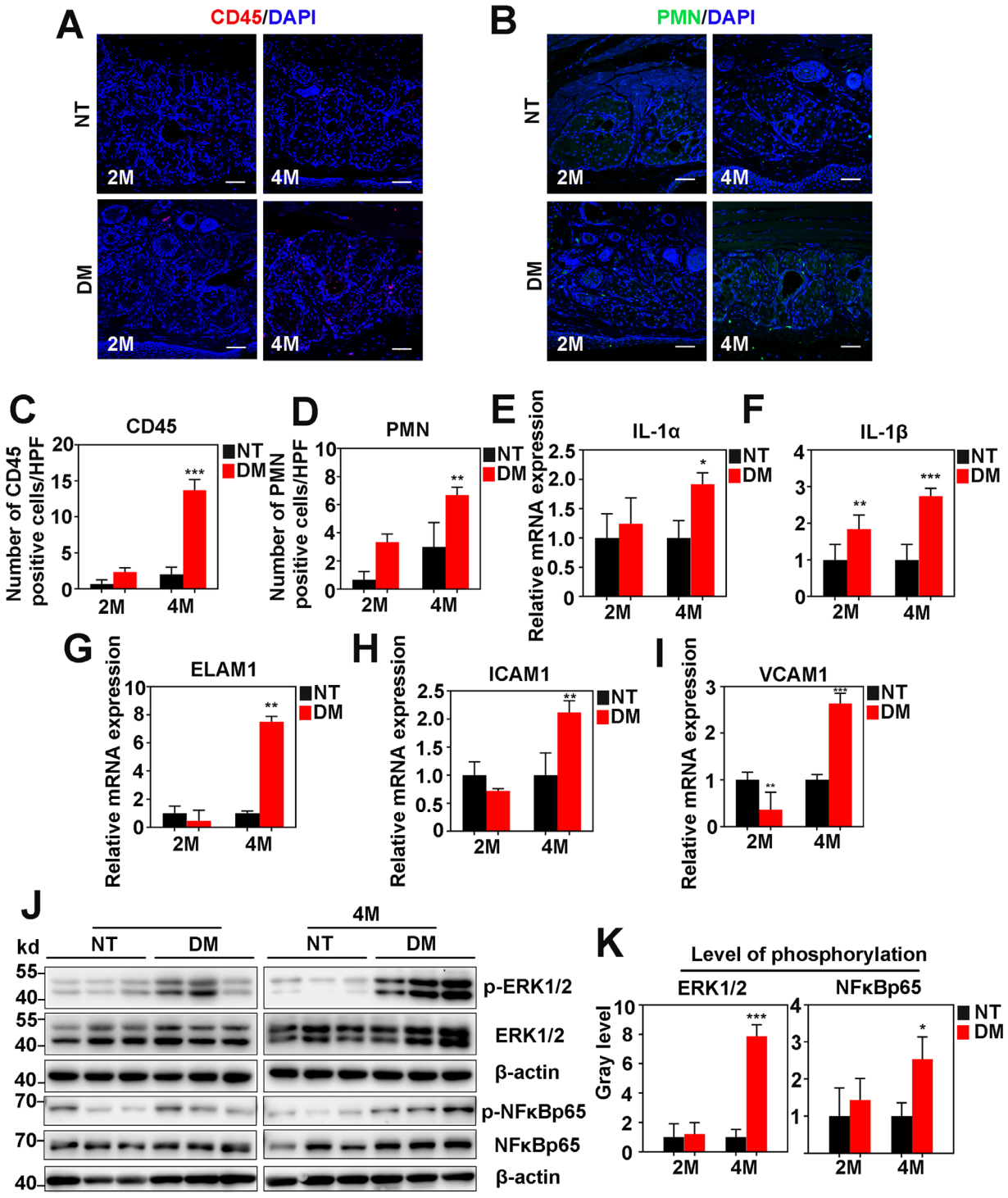

Figure 4. Inflammation of the MG in DM rats. (**A**) Immunofluorescent staining shows CD45 positive cells in the MG. (**B**) Immunofluorescent staining shows PMNs in the MG. (**C**) CD45 positive cell counting shows a significant increase in the 4-month DM group ($n = 3$). (**D**) Quantification of PMN positive cells shows an obvious increase in the 4-month DM group ($n = 3$). (**E–I**) The relative mRNA expression of inflammatory cytokines and adhesion molecules IL-1α, IL-1β, ELAM1, ICAM1, and VCAM1 ($n = 4$). (**J**) The protein expression of pERK1/2, ERK1/2, pNFκB p65, and NFκB p65 in the MG. (**K**) The gray-scale analysis of relative phosphorylation of ERK1/2 and NFκB p65 shows upregulated phosphorylation of ERK1/2 and NFκB p65 in the MG of 4-month DM rats ($n = 3$). $^{*}P < 0.05$, $^{**}P < 0.01$, $^{***}P < 0.001$. Scale bars represent 100 µm in **A** and **B**.

Supplementary Fig. S4F), which was inconsistent with other studies.[42,43] After 2-month metformin gavage, the morphology of the MG was relatively well-maintained (Figs. 6E, 6F), and the acini of rats applied Met for 2 months (the Met4M group) displayed normal structure as the normal control (NT4M) group (Fig. 6G). The ORO staining revealed that lipid accumulation in the MG was widely alleviated in theMet4M group compared with the 4-month DM group

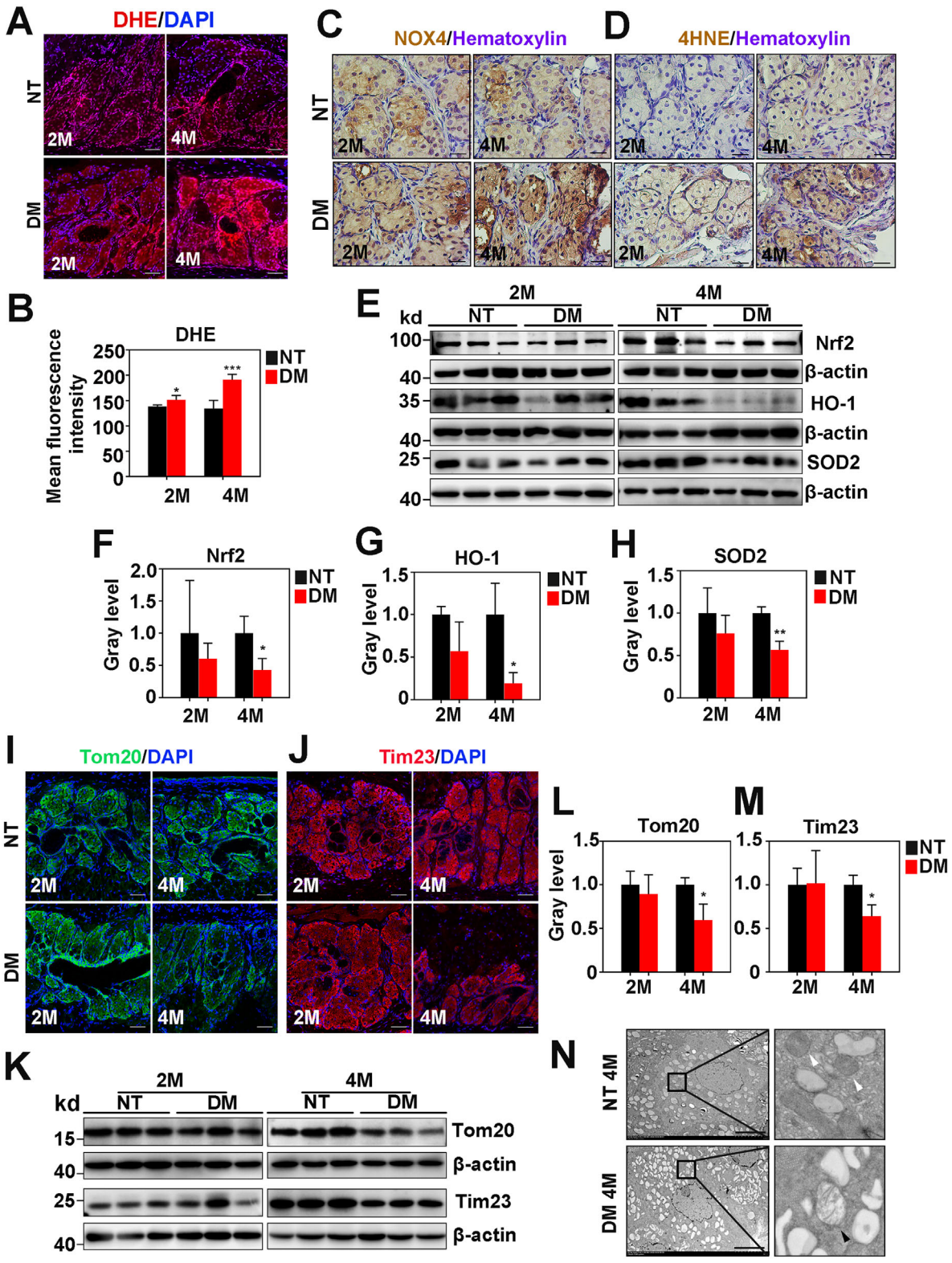

Figure 5. Oxidative stress and mitochondria deterioration of MG in 4-month DM rats. (**A**) Immunofluorescent staining of DHE in the MG. (**B**) The mean fluorescence intensity of DHE in the MG shows upregulation of DHE in the MG of DM rats ($n = 4$). (**C**) Immunohistochemical staining of NOX4 in the MG shows an obvious increase in the 4-month DM group. (**D**) Immunohistochemical staining shows an obvious increase of 4HNE in the MG in the 4-month DM group. (**E**) Western blot analysis of Nrf2, HO-1, and SOD2 in the MG of each group. (**F–H**) The gray-scale analysis of Nrf2, HO-1, and SOD2 protein expression in the MG ($n = 3$). (**I**) Immunofluorescent staining of Tom20 in the MG shows an evident decrease in the 4-month DM group. (**J**) Immunofluorescent staining of Tim23 in the MG shows an evident decrease in the 4-month DM group. (**K**) The protein expression of Tom20 and Tim23 in MG. (**L, M**) The gray-scale analysis of Tom20 and Tim23 in the MG of each group ($n = 3$). (**N**) The transmission electron microscopic images of acinar cells of each group. $^{*}P < 0.05$, $^{**}P < 0.01$, $^{***}P < 0.001$. Scale bars represent 100 µm in **A**, **I**, and **J**, and 50 µm in **C** and **D**, and 5.0 µm in **N**.

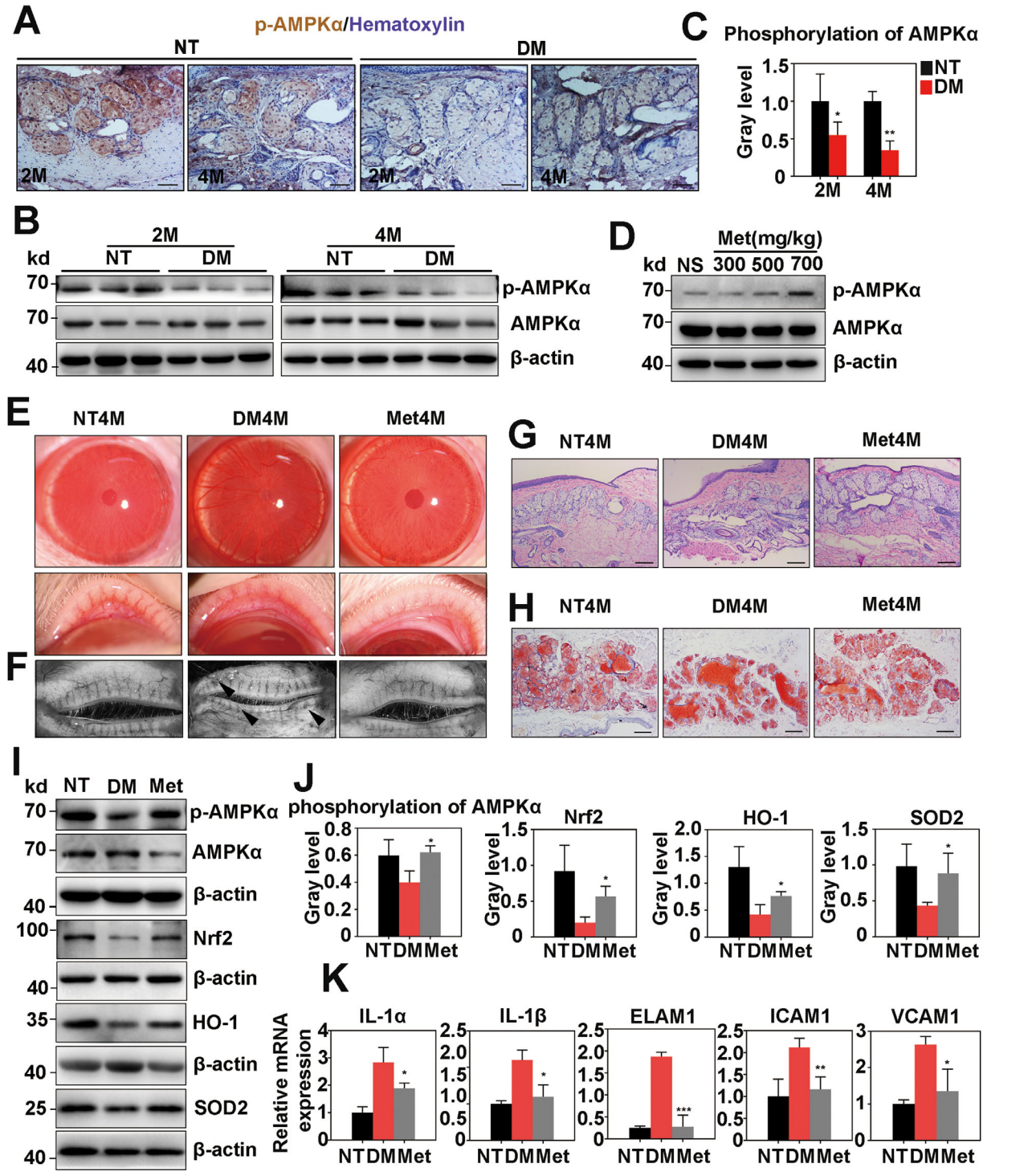

Figure 6. AMPK agonist treatment protects MG from pathological exacerbation in 4-month DM rats. (**A**) Immunohistochemical staining of phospho-AMPKα in the MG shows obvious decrease in the 2-month DM group and the 4-month DM group. (**B**) Western blot analysis results of phospho-AMPKα and AMPKα in the MG. (**C**) The gray-scale analysis of relative phosphorylation of AMPKα shows reduced phospho-AMPKα in the MG of DM rats ($n = 3$). (**D**) Dose response of phospho-AMPKα and AMPKα expression on metformin treatment in the MG. (**E**) Slit lamp images of the ocular surface and the MG after metformin treatment. (**F**) The stereoscopic images of the MG after metformin treatment (*black arrowhead* shows the MG acini dropout in DM rats). (**G**) H&E staining of the MG after metformin treatment. (**H**) ORO staining of the MG after metformin treatment. (**I**) Protein expression level of phospho-AMPKα, AMPKα, Nrf2, HO-1, and SOD2 after metformin treatment. (**J**) The gray-scale analysis of phospho-AMPKα, Nrf2, HO-1, and SOD2 after metformin treatment ($n = 3$). (**K**) The relative mRNA expression of inflammatory cytokines and adhesion molecules IL-1α, IL-1β, ELAM1, ICAM1, and VCAM1 after metformin treatment ($n = 3$). $^{*}P < 0.05$, $^{**}P < 0.01$, $^{***}P < 0.001$. Scale bars represent 100 µm in **A** and 200 µm in **G** and **H**.

Investigative Ophthalmology & Visual Science

(Fig. 6H). Western blot analysis showed that the expression of phospho-AMPKα in the MG was obviously upregulated after Met treatment (Fig. 6I). Simultaneously, the protein expression of anti-oxidation factors Nrf2, HO-1, and SOD2 of the MG in met4M group was clearly increased (Fig. 6I), and confirmed by gray-scale analysis (Fig. 6J). Inflammatory cytokines IL-1α, IL-1β, ELAM1, ICAM1, and VCAM1 were also overtly reduced after metformin treatment (Fig. 6K). These results apparently implied that application of AMPK agonist metformin at the early period of diabetes could protect the MG from MGD induced by hyperglycemia.

Discussion

The TFOS DEWS II Epidemiology Report in 2017 claimed that diabetes was a risk factor of dry eye disease.[8] There have also been plentiful clinical observations that showed that patients with DM were predisposed to MGD, and longer duration of type 2 diabetes is associated with major symptoms and changes in the MG.[12–15] Besides the type 2 DM, recently, a study[44] showed that children with type I DM displayed the shorter tear film break up time than children without DM. These findings implied that hyperglycemia may contribute to the pathology of MGD. However, the pathological process of MGD induced by DM remains elusive, and the therapeutic target is also untouched. Here, for the first time, we determined the correlation between hyperglycemia and MGD and observed the pathological process of MGD induced by diabetes in vivo by means of an STZ induced diabetic rat model. The MG morphology in DM rats changed with the passage of modeling time, which displayed shrunken acini, destroyed acini basement membrane, and disorganized MG structure and MGs dropout. We noticed that the MG pathological changes became obvious around 4 months after STZ application, and there was no MG cell apoptosis and MG acinar change at 1 week and 2 weeks, and the lipid secretion pattern was normal (see Supplementary Figs. S1A, S1B), supported the notion that the MG abnormality was resulted from hyperglycemia rather than direct toxic effect of STZ on MG cells.

We further detected the lipid distribution in MG, which showed the obvious lipid accumulation in the MG of the 4-month DM group. On the other hand, the expression of enzymes related to lipid metabolism of meibum and the pivotal transcriptional factor PPAR-γ involved in lipid metabolism were proved significantly decreased in the MG of the 4-month DM group. We found that the lipid synthesis was relatively normal in response to high glucose at the early stage of DM around 2 weeks. Nevertheless, with the DM prolonged, the keratinization of ductal cells and abnormal differentiation of the MG acinar cells caused the obstruction of ducts, which in turn influenced the lipid discharge ulteriorly led to lipid accumulation and lipid metabolism disorder.

It was reported that diabetes was associated with a state of chronic low-level inflammation.[45] Inflammation was identified as the factor which worsened renal function in patients with diabetes.[46] Diabetes also induces changes in blood vessels and chronic inflammation in the retina and eventually caused retinal ganglion cell loss.[47] Our data showed apparently increased inflammatory cells infiltration and significant elevated inflammatory cytokines expression in the MG of DM rats. ERK1/2 NF-κB plays an important role in regulating inflammatory responses.[30,31] The obvious activation of ERK1/2 and NF-κB p65 in the MG of the 4-month DM group indicated the inflammatory microenvironment of the MG under diabetic conditions.

Oxidative stress was regarded as the most crucial pathology in diabetes. Free radicals generated by autoxidation reactions of advanced glycation end-products (AGEs) to protein and unsaturated lipids in plasma and membrane accumulated in tissue collagen in diabetes and further exacerbated the oxidative stress.[48,49] It was noteworthy that the ROS level was evidently increased in the MG of 2-month DM rats, indicating the early production of excessive ROS in the MG. However, the expression of NOX4 and 4HNE was increased in the MG of the 4-month DM group, meanwhile the expression of anti-oxidation factor Nrf2, HO-1, and SOD2 was decreased in the MG of the 4-month DM group, and the mitochondrion of MG deteriorated in the 4-month DM group, which implied that over production of ROS in the early stage of DM might be the initial factor for the pathology of MGD induced by hyperglycemia.

It was known that AMPK played the central role in the metabolism.[36] Numerous studies have reported that inactivation of AMPK is involved in the pathology of diabetes.[37,50] Our study also found downregulation of p-AMPKα as early as 2 months after STZ induction, which was concurrent with over production of ROS. Therefore, we postulated that AMPK agonist, such as Met could activate AMPK signaling pathway in the MG in the early stage of DM and protect the MG from deteriorative pathological change. It was interesting to note that Met took its effect at 700 mg/kg in MG by p-AMPKα dose response, which was comparatively higher than the common dosage utilized in other organs and tissues.[39–41] After the 2-month metformin gavage, we found that the morphology of the MG in the Met group was much more ameliorated than the 4-month DM group with normal saline gavage, lipid accumulation also decreased to the normal group level. On the other hand, anti-oxidation factors, such as Nrf2, HO-1, and SOD2, showed evident upregulation and inflammatory cytokines as well as adhesion molecules showed overt downregulation after Met treatment. These results indicated validity of Met in MGD induced by hyperglycemia. It was worth noting that there was no significant drop of blood glucose level after Met treatment in the DM group, suggesting that Met ameliorated MGD through activation of AMPK signaling pathway instead of reducing the blood glucose.

Based on our results, the excessive production of ROS in the MG induced by hyperglycemia led to severe oxidative stress, along with inflammation, abnormal cell differentiation, and keratinization, contributed to the pathological changes of MG induced by hyperglycemia. However, whether oxidative stress caused by excessive ROS was the initial factor during the whole process needs definite evidence and further investigation. In addition to MGs, the state of the ocular surface in the 4-month DM group was evaluated. The tear secretion of 4-month DM rats showed an evident decrease (see Supplementary Fig. S4E), as shown in previous studies.[51,52] However, there were no obvious corneal defects and corneal keratinization in 4-month DM rats. Therefore, the Meibomian gland drop out and lacrimal gland change may not cause the obvious corneal and conjunctiva change. Corneal and conjunctival tissues could compensate at an early stage of DM. Observation for longer duration is necessary in future study. As shown in the previous study that dry eye syndrome worsens with the duration of diabetes.[53] In summary, we identified that long-term diabetes could induce acini apoptosis, abnormal cell differentiation, ductal and acini keratinization, lipid metabolism

Investigative Ophthalmology & Visual Science

disorder, inflammation, and oxidative stress in the MG, which were consistent with characteristics of MGD. The diabetic rat model may be used as the MGD model for studying the correlation between MGD and glucose metabolic disorder. Moreover, we indicated that AMPK was inactivated in MG at the early stage of DM and AMPK agonist metformin could ameliorate the MGD induced by hyperglycemia, which provided evidence for clinical therapeutics of MGD associated with DM.

Acknowledgments

Supported in part by the National Key R&D Program of China (2018YFA0107301 and 2018YFA0107304), the National Natural Science Foundation of China (NSFC; No. 81770894, No. 81470602, No. 81970773, and No. 81870625).

Disclosure: **Y. Guo,** None; **H. Zhang,** None; **Z. Zhao,** None; **X. Luo,** None; **M. Zhang,** None; **J. Bu,** None; **M. Liang,** None; **H. Wu,** None; **J. Yu,** None; **H. He,** None; **R. Zong,** None; **Y. Chen,** None; **Z. Liu,** None; **W. Li,** None

References

1. Jester JV, Nicolaides N, Smith RE. Meibomian gland studies: histologic and ultrastructural investigations. *Invest Ophthalmol Vis Sci*. 1981;20:537–547.
2. Willcox MDP, Argüeso P, Georgiev GA, et al. TFOS DEWS II Tear Film Report. *Ocular Surface*. 2017;15:366–403.
3. Butovich IA. Meibomian glands, meibum, and meibogenesis. *Exp Eye Res*. 2017;163:2–16.
4. Nelson JD, Shimazaki J, Benitez-del-Castillo JM, et al. The international workshop on meibomian gland dysfunction: report of the definition and classification subcommittee. *Invest Ophthalmol Vis Sci*. 2011;52:1930–1937.
5. Chhadva P, Goldhardt R, Galor A. Meibomian Gland Disease: The Role of Gland Dysfunction in Dry Eye Disease. *Ophthalmology*. 2017;124:S20–S26.
6. Sullivan DA, Sullivan BD, Evans JE, et al. Androgen deficiency, Meibomian gland dysfunction, and evaporative dry eye. *Ann N Y Acad Sci*. 2002;966:211–222.
7. Bu J, Wu Y, Cai X, et al. Hyperlipidemia induces meibomian gland dysfunction. *Ocular Surface*. 2019;17:777–786.
8. Stapleton F, Alves M, Bunya VY, et al. TFOS DEWS II Epidemiology Report. *Ocular Surface*. 2017;15:334–365.
9. Vieira-Potter VJ, Karamichos D, Lee DJ. Ocular Complications of Diabetes and Therapeutic Approaches. *BioMed Res Intl*. 2016;2016:3801570.
10. Najafi L, Malek M, Valojerdi AE, et al. Dry eye and its correlation to diabetes microvascular complications in people with type 2 diabetes mellitus. *J Diabetes Complications*. 2013;27:459–462.
11. Jan RL, Tai MC, Ho CH, et al. Risk of recurrent corneal erosion in patients with diabetes mellitus in Taiwan: a population-based cohort study. *BMJ Open*. 2020;10:e035933.
12. Lin X, Xu B, Zheng Y, et al. Meibomian Gland Dysfunction in Type 2 Diabetic Patients. *J Ophthalmol*. 2017;2017:3047867.
13. Yu T, Shi WY, Song AP, Gao Y, Dang GF, Ding G. Changes of meibomian glands in patients with type 2 diabetes mellitus. *Int J Ophthalmol*. 2016;9:1740–1744.
14. Yu T, Han XG, Gao Y, Song AP, Dang GF. Morphological and cytological changes of meibomian glands in patients with type 2 diabetes mellitus. *Int J Ophthalmol*. 2019;12:1415–1419.
15. Shamsheer RP, Arunachalam C. A Clinical Study of Meibomian Gland Dysfunction in Patients with Diabetes. *Middle East African J Ophthalmol*. 2015;22:462–466.
16. Ding J, Liu Y, Sullivan DA. Effects of Insulin and High Glucose on Human Meibomian Gland Epithelial Cells. *Invest Ophthalmol Vis Sci*. 2015;56:7814–7820.
17. Furman BL. Streptozotocin-Induced Diabetic Models in Mice and Rats. *Curr Protocols Pharmacol*. 2015;70:5.47.41–45.47.20.
18. Craig JP, Nichols KK, Akpek EK, et al. TFOS DEWS II Definition and Classification Report. *Ocular Surface*. 2017;15:276–283.
19. Butovich IA, McMahon A, Wojtowicz JC, Lin F, Mancini R, Itani K. Dissecting lipid metabolism in meibomian glands of humans and mice: An integrative study reveals a network of metabolic reactions not duplicated in other tissues. *Biochimica et Biophysica Acta*. 2016;1861:538–553.
20. Butovich IA, Wilkerson A, Bhat N, McMahon A, Yuksel S. On the pivotal role of Elovl3/ELOVL3 in meibogenesis and ocular physiology of mice. *FASEB Journal: Official Publication of the Federation of American Societies for Experimental Biology*. 2019;33:10034–10048.
21. Butovich IA, Wilkerson A, Yuksel S. Depletion of Cholesteryl Esters Causes Meibomian Gland Dysfunction-Like Symptoms in a Soat1-Null Mouse Model. *Int J Mol Sci*. 2021;22:1583.
22. Trivedi NR, Cong Z, Nelson AM, et al. Peroxisome proliferator-activated receptors increase human sebum production. *J Invest Dermatol*. 2006;126:2002–2009.
23. Nien CJ, Paugh JR, Massei S, Wahlert AJ, Kao WW, Jester JV. Age-related changes in the meibomian gland. *Exp Eye Res*. 2009;89:1021–1027.
24. Nien CJ, Massei S, Lin G, et al. Effects of age and dysfunction on human meibomian glands. *Arch Ophthalmol (Chicago, Ill : 1960)*. 2011;129:462–469.
25. Senoo M, Pinto F, Crum CP, McKeon F. p63 Is essential for the proliferative potential of stem cells in stratified epithelia. *Cell*. 2007;129:523–536.
26. Knop E, Knop N, Millar T, Obata H, Sullivan DA. The international workshop on meibomian gland dysfunction: report of the subcommittee on anatomy, physiology, and pathophysiology of the meibomian gland. *Invest Ophthalmol Vis Sci*. 2011;52:1938–1978.
27. Jester JV, Rife L, Nii D, Luttrull JK, Wilson L, Smith RE. In vivo biomicroscopy and photography of meibomian glands in a rabbit model of meibomian gland dysfunction. *Invest Ophthalmol Vis Sci*. 1982;22:660–667.
28. Smith F. The molecular genetics of keratin disorders. *Am J Clin Dermatol*. 2003;4:347–364.
29. Li S, Nikulina K, DeVoss J, et al. Small proline-rich protein 1B (SPRR1B) is a biomarker for squamous metaplasia in dry eye disease. *Invest Ophthalmol Vis Sci*. 2008;49:34–41.
30. Lu N, Malemud CJ. Extracellular Signal-Regulated Kinase: A Regulator of Cell Growth, Inflammation, Chondrocyte and Bone Cell Receptor-Mediated Gene Expression. *Int J Mol Sci*. 2019;20:3792.
31. Wullaert A, Bonnet MC, Pasparakis M. NF-κB in the regulation of epithelial homeostasis and inflammation. *Cell Res*. 2011;21:146–158.
32. Maritim AC, Sanders RA, Watkins JB, 3rd. Diabetes, oxidative stress, and antioxidants: a review. *J Biochem Molec Toxicol*. 2003;17:24–38.
33. Bedard K, Krause KH. The NOX family of ROS-generating NADPH oxidases: physiology and pathophysiology. *Physiolog Rev*. 2007;87:245–313.
34. Zorov DB, Juhaszova M, Sollott SJ. Mitochondrial reactive oxygen species (ROS) and ROS-induced ROS release. *Physiolog Rev*. 2014;94:909–950.
35. Li A, Zheng N, Ding X. Mitochondrial abnormalities: a hub in metabolic syndrome-related cardiac dysfunction caused

by oxidative stress [published online May 5, 2021]. *Heart Fail Rev*, https://doi.org/10.1007/s10741-021-10109-6.

36. Herzig S, Shaw RJ. AMPK: guardian of metabolism and mitochondrial homeostasis. *Nat Rev Molec Cell Biol*. 2018;19:121–135.
37. Madhavi YV, Gaikwad N, Yerra VG, Kalvala AK, Nanduri S, Kumar A. Targeting AMPK in Diabetes and Diabetic Complications: Energy Homeostasis, Autophagy and Mitochondrial Health. *Curr Medicinal Chem*. 2019;26:5207–5229.
38. Foretz M, Guigas B, Bertrand L, Pollak M, Viollet B. Metformin: from mechanisms of action to therapies. *Cell Metabolism*. 2014;20:953–966.
39. Balamash KS, Alkreathy HM, Al Gahdali EH, Khoja SO, Ahmad A. Comparative Biochemical and Histopathological Studies on the Efficacy of Metformin and Virgin Olive Oil against Streptozotocin-Induced Diabetes in Sprague-Dawley Rats. *J Diabetes Res*. 2018;2018:4692197.
40. Yarat A, Yanardağ R, Tunali T, et al. Effects of glibornuride versus metformin on eye lenses and skin in experimental diabetes. *Arzneimittel-Forschung*. 2006;56:541–546.
41. Yang S, Lv Q, Luo T, et al. Metformin inhibits expression and secretion of PEDF in adipocyte and hepatocyte via promoting AMPK phosphorylation. *Mediators of Inflammation*. 2013;2013:429207.
42. Nahar N, Mohamed S, Mustapha NM, Lau S, Ishak NIM, Umran NS. Metformin attenuated histopathological ocular deteriorations in a streptozotocin-induced hyperglycemic rat model. *Naunyn-Schmiedeberg's Archives of Pharmacology*. 2021;394:457–467.
43. Kassab BM, Hussein HH, Mahmoud OM, Abdel-Alrahman G. Effects of insulin and metformin on fetal kidney development of streptozotocin-induced gestational diabetic albino rats. *Anat Cell Biol*. 2019;52:161–175.
44. Wang S, Jia Y, Li T, et al. Dry Eye Disease Is More Prevalent in Children with Diabetes than in Those without Diabetes. *Curr Eye Res*. 2019;44:1299–1305.
45. Wellen KE, Hotamisligil GS. Inflammation, stress, and diabetes. *J Clin Invest*. 2005;115:1111–1119.
46. Turkmen K. Inflammation, oxidative stress, apoptosis, and autophagy in diabetes mellitus and diabetic kidney disease: the Four Horsemen of the Apocalypse. *Int Urology Nephrol*. 2017;49:837–844.
47. Potilinski MC, Lorenc V, Perisset S, Gallo JE. Mechanisms behind Retinal Ganglion Cell Loss in Diabetes and Therapeutic Approach. *Int J Mol Sci*. 2020;21:2351.
48. Baynes JW. Role of oxidative stress in development of complications in diabetes. *Diabetes*. 1991;40:405–412.
49. Forbes JM, Coughlan MT, Cooper ME. Oxidative stress as a major culprit in kidney disease in diabetes. *Diabetes*. 2008;57:1446–1454.
50. Zhang BB, Zhou G, Li C. AMPK: an emerging drug target for diabetes and the metabolic syndrome. *Cell Metabolism*. 2009;9:407–416.
51. Yin J, Huang J, Chen C, Gao N, Wang F, Yu FS. Corneal complications in streptozocin-induced type I diabetic rats. *Invest Ophthalmol Vis Sci*. 2011;52:6589–6596.
52. Liu X, Liu H, Lu X, Zhao S. N-acetylcysteine alleviates ocular surface damage in STZ-induced diabetic mice by inhibiting the ROS/NLRP3/Caspase-1/IL-1β signaling pathway. *Exp Eye Res*. 2021;209:108654.
53. Lyu Y, Zeng X, Li F, Zhao S. The effect of the duration of diabetes on dry eye and corneal nerves. *Contact Lens & Anterior Eye : the Journal of the British Contact Lens Association*. 2019;42:380–385.

Investigative Ophthalmology & Visual Science